CORRELATIVE LIGHT MICROSCOPY AND X-RAY MICROTOMOGRAPHY OF GROUND SECTIONS OF MINERALISED TISSUES.

David Mills, Alan Boyde
Dental Physical Science Unit, Bancroft Building, Queen Mary University of London, London E1 4NS

ABSTRACT

Starting from scratch, if one wanted to correlate light microscopical (LM) and X-ray microtomographic (XMT, micro-CT) findings from the mineralized tissues – bone and calcified cartilage in the skeleton and dentine, enamel, and cementum in teeth – one could simply examine the same, resin embedded sample with at least one flat surface by confocal scanning reflection and/or fluorescence light microscopy and XMT. However, we are frequently presented with ready-made 'ground' sections mounted in Canada balsam or DPX on 25mm wide ~ 1mm thick glass slides with 0.17mm cover slips. Many such preparations are historical or are valuable by representing archival material from rare diseases or endangered species: all are inconvenient in form for XMT. We endeavored to economize on X-ray beam time by scanning a 25mm thick stack of slides, separating the relevant data from each sample and making exact matches with transmitted ordinary and polarized light microscopy images. Samples were selected to represent a wide range of sizes and skeletal and dental tissue types, including human femoral bone, human permanent teeth, dog carnassial tooth, narwhal mandible, black rhinoceros molars, sperm whale cementum and dentine, African elephant ivory, and prairie marmot molars. XMT was conducted using the QMUL Mucat-2 system [1], nominal voxel size 20μm, 90kV, 24 hours. Analysis used in-house analysis software TomView, ImageJ [2] and Drishti [3] software. In each case we were able to match XMT and light microscopy. We can now report mineralization densities for all the calcified tissues in the context of classical light microscopy imagery.

Keywords: light microscopy, linear attenuation coefficient, calcified tissues, histology, x-ray microtomography, micro-ct

1. INTRODUCTION

X-ray microtomography (XMT) was introduced for the study of dental and skeletal tissues by Elliott and Dover (1982) [4], primarily for the non-destructive measurement of X-ray absorption coefficient in mineralised tissues.The development of the method in our QMUL laboratory since then has continued to focus on the provision of accurate and reliable estimates of mineral concentration in the hard tissues [5-15].

Today, XMT is extremely widespread with large numbers of commercial, mainly high throughput systems available and in use: searching PubMed on 'X-ray microtomography and bone' shows 7137 papers, with the rapid take-up after 2009. 'X-ray microtomography and teeth' scores 1825 results. 'Micro-CT and (bone or teeth)' scores 12058. XMT is therefore now widely known and very popular.

However, we have been unable to find a single instance in the literature of the XMT investigation of existing, undecalcified, 'ground' sections of calcified tissues mounted for conventional light microscopy – even though there is, worldwide, a large stock of such material in established hard tissue research laboratories and museums. Reasons for being interested in such material include their historic or scientific significance, that they have been studied by special methodologies, or that they have been produced from material from rare or extinct species or rare disease conditions, and thus contain material that is irreplaceable, given the changes in attitude and restrictions in access to research material which have evolved in recent decades. Digital microscopy techniques can be employed to produce high-quality, high-resolution images of the tissues on a slide with a variety of modalities including polarized light (PLM), phase contrast and differential interference contrast, and confocal reflection and fluorescence, but none of these allow quantification of mineralization of the tissues. We wanted to provide that correlation.

2. MATERIALS AND METHODS

A typical light microscopic preparation is composed of a 75mm x 25mm x 1mm soda-lime glass slide with a composition of approximately 75% SiO2, 15% Na2O and 10% CaO [Empirical formula = Ca_2, Na_5, O_{30}, Si_{13}]: the specimen is mounted on the slide in either Canada balsam or DPX and covered with a 170µm thickness coverslip of borosilicate glass.

Slides were selected based on current interest, whether the slide was of material from a rare or endangered species and the type and number of tissues present.

Table 1: List of Slides with Identifying Details used in this study. The full data set can be found at [16].

Slide ID	Sample Details
A	Narwhal mandibular condyle 1-10-98
B	African elephant, *Loxodonta*, tusk ivory transverse section
C	Two human upper first premolars, bucco-palatal longitudinal sections with shallow grooves & 'fissure sealant' composite [Broken slide]
D	Bone section. Anatomy Dept UCL loan slide box 35 slide 67
E	Walrus tusk, transverse section
F	Savanna elephant (Sudan 1902) ivory ground section, British Museum Register number 1941-207
G	Longitudinal labio-lingual ground section human canine
H	Dog carnassial tooth, longitudinal mesio-distal section 11-12-64
I	Sperm whale dentine section used for osteoclastic resorption assay, stained toluidine blue, mounted dry, no cover slip
J	Black rhino, *Diceros bicornis*, tooth transverse section
K	Black rhino, *Diceros bicornis*, tooth transverse section
L	Black rhino, *Diceros bicornis*, tooth longitudinal section
M	Black rhino, *Diceros bicornis*, tooth longitudinal section
N	Human upper canine labio-lingual longitudinal section
O	Prairie marmot, *Cynomys ludivicianus*, molar

For XMT, we used the QMUL MuCAT-2 scanner with the multi-metal calibration carousel and supporting software packages at the X-Ray microtomography facility in the QMUL Dental Institute. This is optimised for tissue mineralisation measurement [17] and is part of a continuous chain of development from the original tomography scanner [18-20]. Fifteen slides were mounted such that the coverslip of one slide touched the back of the next slide. The thickness of the slides and coverslips was found to be uniform enough to enable easy segmentation. The 15 slides produced an approximately square section sample with similar attenuation in all projections. The x-ray settings were 90kV and 180µA, the exposure time was 6 seconds per projection and 2601 projections were collected in each of two non-overlapping adjacent 'blocks' in the rotation axis of the sample.

The reconstructed voxel size was 20µm. The projections were calibrated and corrected for beam-hardening by means of a multi-element calibration carousel, with the assumption the majority material in the scan volume was SiO_2. In the calibrated scan, it was seen that the slides had very similar linear attenuation coefficients (LACs), while there was some significant variation in the LAC of the coverslips. Two coverslips were seen to be particularly radio-opaque, suggesting the use of high refractive index lead glass coverslips. The contribution to the attenuation of the whole volume by these coverslips was judged to be minimal.

It was seen after reconstruction that the slides were not perfectly parallel with each other and not perfectly vertical in the scanner, which made the extraction of an XMT slice directly comparable to the optical image more difficult. This is shown in Figure 1. If care is not taken with post-reconstruction alignment, it hazards a loss of resolution and the introduction of artefacts and especially in such thin samples. To minimise the introduction of artefacts, the projections were reconstructed again at two-fold magnification, aligned and down-sampled to original size. Alignment and down-sampling was performed for each slide to produce a plane parallel surface which could be compared to the visible light microscopy.

To measure the LAC, the volumetric data was exported from TomView to a 'stack' in ImageJ. In the case of solid samples, the first and last slices in the sample volume were removed to avoid partial volume effects and then the remaining voxel values in the thickness of the sample were averaged. (In the case of samples of uneven thickness, sufficient voxel layers were removed from each side of the stack to ensure that the voxels used for the average were entirely inside the stack). For

porous samples - trabecular bone - the same process was applied, but additionally the bone was masked and eroded in ImageJ to remove one voxel from all trabecular surfaces to avoid partial volume effects.

In a single or two material volume where the composition of the materials is known it is possible to calculate the density of the material from the measured LAC using the following equation, assuming the mass attenuation coefficient (MAC) for each material is known or can be computed.

$$\rho = \frac{LAC}{MAC}$$

We did not have this simple case, because we have different natural calcified tissues which by their nature will exhibit some non-ideal and difficult to compute MACs [21]. We instead used the fact the majority material in the scanned volume was soda-lime glass with a broadly known composition, calculated the expected LAC using the XCOM [22] database and used this to calibrate the measured LACs. The calculated LAC for soda-lime glass under our scanning, beam hardening correction and calibration conditions was 1.3cm^{-1}.

For a low magnification optical image overview, the slides were imaged with a Plustek OpticFilm 8100 35mm film scanner with a carrier modified to accept standard glass microscope slides. VueScan software control of the scanner allowed imaging at 7200 DPI corresponding to a pixel size of 3.53µm. They were also imaged at higher magnifications with a novel PLM using digitally controlled rotating crossed polarisers to enable determination of the orientation of birefringent microstructure in three dimensions [23].

3. RESULTS

Examples of the XMT and optical images from this study are shown in Figures 1-5 and details of features of interest are given in the captions.

The average measured LAC for the glass slides was 1.2cm^{-1} suggesting that our measured LAC values for the samples will be ~8% low. Table 2 gives the measured minimum, maximum and mean measured LAC values and the mean value corrected by 8%. A minimum of three voxels in the thickness of the sample is required to produce a value for LAC: more voxels allow for more averaging. Some of the samples were too thin to produce reliable LAC values, so they are not presented here.

Table 2: LAC values measured from the XMT data, units are cm^{-1}

Slide ID	Sample Details	LAC_{min}	LAC_{max}	LAC_{mean}	$LAC_{corrected}$
A	Trabecular bone in narwhal mandibular condyle	0.70	1.38	1.21	1.31
B	African elephant ivory, dentine & cementum	0.98	1.45	1.23	1.34
C	Human upper first premolars - enamel	1.56	2.00	1.79	1.94
C	Human upper first premolars - dentine	0.94	1.30	1.12	1.22
E	Walrus tusk, dentine & cementum	0.78	1.34	1.15	1.25
H	Dog carnassial tooth - enamel	1.48	1.97	1.83	1.99
H	Dog carnassial tooth - dentine	0.86	1.37	1.18	1.23
I	Sperm whale dentine & cementum	0.81	1.33	1.18	1.28
J	Black rhino TS - dentine	1.12	1.42	1.29	1.40
J	Black rhino TS - enamel	1.60	1.93	1.77	1.91
K	Black rhino LS - enamel	1.81	2.16	2.00	2.16
K	Black rhino LS - dentine	1.12	1.56	1.37	1.49
N	Human upper canine - enamel	1.85	2.21	2.05	2.21
N	Human upper canine - dentine	1.16	1.42	1.31	1.42

4. DISCUSSION

XMT – the abbreviation we use in house, albeit that μCT or micro-CT are also in common usage and more effective as search terms – has now been around for nearly four decades and is now in common use for studies of calcified tissues [4-15, 24-26]. The present study shows for the first time that it is possible to use XMT to obtain LAC values related to mineralization of the sample on batches of existing, archival microscopic slide preparations. However, conversion of the recovered LAC values to material density requires deeper knowledge of the composition of the sample so the MAC of the material can be calculated. Ground sections of calcified tissues prepared for transmitted light microscopy are by their nature very thin - light must be able to pass through them. On the other hand, XMT produces the best results with thicker samples and more voxels in the thickness of the sample allows a more accurate estimation of the LAC. Scanning slides at higher spatial resolution would give a larger number of voxels, but at the cost of significantly longer scan times and smaller field of view. Long scans might also come with the issue of higher integrated radiation flux, possibly leading to color-center formation, and darkening of the glass.

Reconstruction of the data at double size and then down-sampling after alignment allows a very good match between the tomography and the optical microscopy. In a continuation of this work, we are trialing special holders which will keep multiple LM slides parallel so that we can obtain substantial XYZ data sets without any complex data manipulation.

5. REFERENCES

[1] Evershed ANZ, Mills D and Davis GR, "Multi-species beam hardening calibration device for x-ray microtomography", 85061N-85061N – 12, Proceedings Volume 8506, Developments in X-Ray Tomography VII (2012).

[2] Schindelin J, Arganda-Carreras I, Frise E, Kaynig V, Longair M, Pietzsch T, Preibisch S, Rueden C, Saalfeld S, Schmid B, Tinevez JY, White DJ, Hartenstein V, Eliceiri K, Tomancak P and Cardona A, "Fiji: an open-source platform for biological-image analysis", Nature Methods 9(7), 676–682 (2012).

[3] Limaye A, "Drishti: a volume exploration and presentation tool", Proceedings Volume 8506, Developments in X-Ray Tomography VIII (2012).

[4] Elliott JC and Dover SD, "X-ray microtomography", J Microscopy 126(2), 211–213 (1982).

[5] Elliott JC and Dover SD, "Three-dimensional distribution of mineral in bone at a resolution of 15 μm determined by x-ray microtomography", Metabolic Bone Dis Relat Res 5(5), 219–221 (1984).

[6] Elliott JC, Bowen DK, Dover SD and Davies ST, "X-ray microtomography of biological tissues using laboratory and synchrotron sources", Biol Trace Elem Res 13(1), 219–227 (1987).

[7] Mechanic GL, Arnaud SB, Boyde A, Bromage TG, Buckendahl P, Elliott JC, Katz EP. and Durnova GN, "Regional distribution of mineral and matrix in the femurs of rats flown on Cosmos 1887 biosatellite", FASEB J 4(1), 34–40 (1990).

[8] Elliott JC, Anderson P, Davis GR., Wong FSL, Gao XJ, Dover SD and Boyde A, "X-ray microtomographic studies of bones and teeth", Springer Series in Optical Sciences, 461–464 (1992).

[9] Fearne JM, Elliott JC, Wong FSL, Davis GR, Boyde A and Jones SJ, "Deciduous enamel defects in low-birth-weight children: correlated X-ray microtomographic and backscattered electron imaging study of hypoplasia and hypomineralization", Anat Embryol 189(5), 375–381 (1994).

[10] Wong FSL, Elliott JC, Anderson P and Davis GR, "Mineral concentration gradients in rat femoral diaphyses measured by X-ray microtomography", Calcified Tissue Int 56(1), 62–70 (1995).

[11] Davis GR and Wong F, "X-ray microtomography of bones and teeth", Physiol Meas 17(3), 121–146 (1996).

[12] Anderson P, Elliott JC, Bose U and Jones SJ, "A comparison of the mineral content of enamel and dentine in human premolars and enamel pearls measured by X-ray microtomography", Arch Oral Biol 41(3), 281–290 (1996).

[13] Elliott JC, Anderson P, Davis GR, Wong FSL, Dowker SEP, Kozul N and Boyde A, “Microtomography in medicine and related fields”, Developments in X-ray Microtomography, 2–12 (1997).

[14] Davis GR, Elliott JC, Anderson P, Wouters K, Procter P, Boyde A, “Rapid prototyping of a high resolution x-ray microtomographic image data set showing trabecular bone within a human vertebral body”, Scanning 19, 175–177 (1997).

[15] Davis GR, Dowker SEP, Elliott JC, Anderson P, Wassif HS, Boyde A, Goodship AE, Ignatiev SRS and Ignatiev K, “Non-destructive 3D structural studies by X-ray microtomography”, Proceedings of the 50th Annual Denver X-ray Conference 45, Huang TC, Ed., 485–490 (2001).

[16] Mills D and Boyde A, “SPIE 2021 Data”, <https://figshare.com/collections/SPIE_2021/5532303> (Accessed 3 September 2021).

[17] Davis GR, Evershed ANZ and Mills D, “Characterisation of materials: Determining density using X-ray microtomography”, Materials Science and Technology 31(2), 162–166 (2015).

[18] Davis GR and Elliott JC, “X-ray microtomography scanner using time-delay integration for elimination of ring artefacts in the reconstructed image”, Nuclear Instruments and Methods in Physics Research Section A: Accelerators, Spectrometers, Detectors and Associated Equipment 394 (1–2), 157–162 (1997).

[19] Davis G. and Elliott JC, “High definition X-ray microtomography using a conventional impact X-ray source”, J De Physique IV Proc 104, 131–134 (2003).

[20] Davis G, Evershed A, Elliott JC, and Mills D, “Quantitative X-ray microtomography with a conventional source”, 78040I-78040I – 8, Developments in X-Ray Tomography VII. (2010)

[21] Herkströter FM and Bosch JJT, “Wavelength-independent Microradiography: A Method for Non-destructive Quantification of Enamel and Dentin Mineral Concentrations using Polychromatic X-rays”, J Dent Res 69(8), 1522–1526 (1990).

[22] Berger MJ, Seltzer SM, Chang J, Coursey JS, Sukumar R, Zucker DS, Olsen K., “XCOM: Photon Cross Section Database (version 1.5)”, <http://physics.nist.gov/xcom> (Accessed 3 September 2021).

[23] Boyde A, Felder A, Mills D, “New approach to increase information content in polarised light microscopy of skeletal and dental tissues”, https://www.mmc-series.org.uk/general-information/previous-congresses/mmc2019-scientific-programme.html (2019)

[24] Bonse U, Busch F, Günnewig O, Beckmann F, Pahl R, Delling G, Hahn M. and Graeff W, “3D computed X-ray tomography of human cancellous bone at 8μm spatial and 10−4 energy resolution”, Bone Miner 25(1), 25–38 (1994).

[25] Engelke K, Graeff W, Meiss L, Hahn M And Delling G, “High Spatial Resolution Imaging of Bone Mineral Using Computed Microtomography”, Invest Radiol 28(4), 341–349 (1993).

[26] Yasumura S, Jones K, Spanne P, Schidlovsky G, Wielopolski L., Ren X, Glaros D. and Xatzikonstantinou Y, “In Vivo Animal Models of Body Composition in Aging”, J Nutrition 123, 459–464 (1993).

[27] Boyde A, Bromage TG. Histology of dental hard tissues. In (de Buffrenil V, de Ricqlès A, Zylberberg L, Padian K, Eds) Vertebrate Skeletal Histology and Paleohistology. CRC Press: London. Section IV Teeth, Chapter 13. (2021).

6. FIGURES

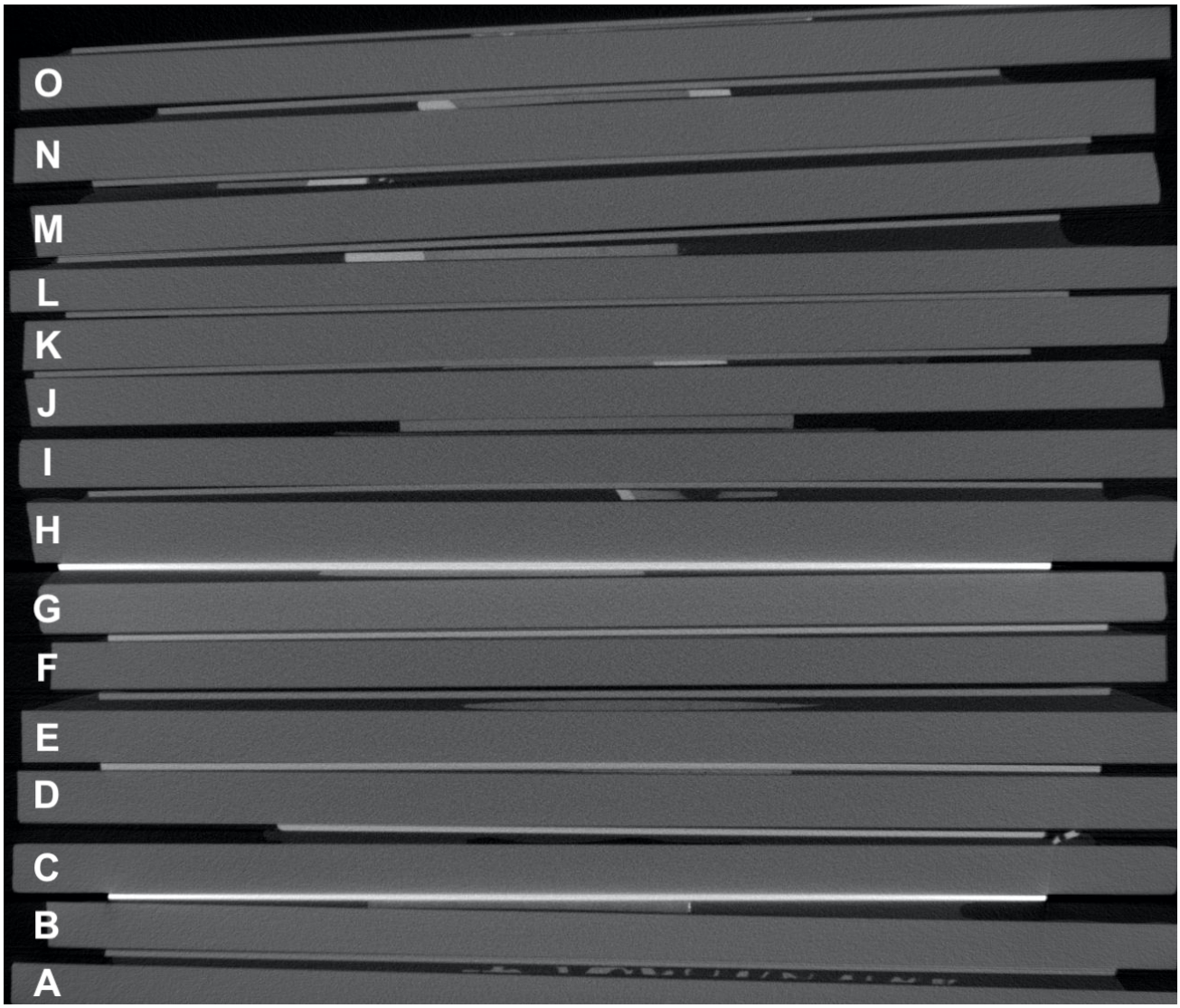

Figure 1: The initial XMT output of the scan of the stack of 15 slides before alignment and segmentation. Two particularly radio-opaque coverslips can be seen for slides B and G which were of unknown origin. Slide I (sperm whale tooth) has no coverslip: the apparent gap between section and slide is occupied by double sided adhesive tape. Total field height is 25mm.

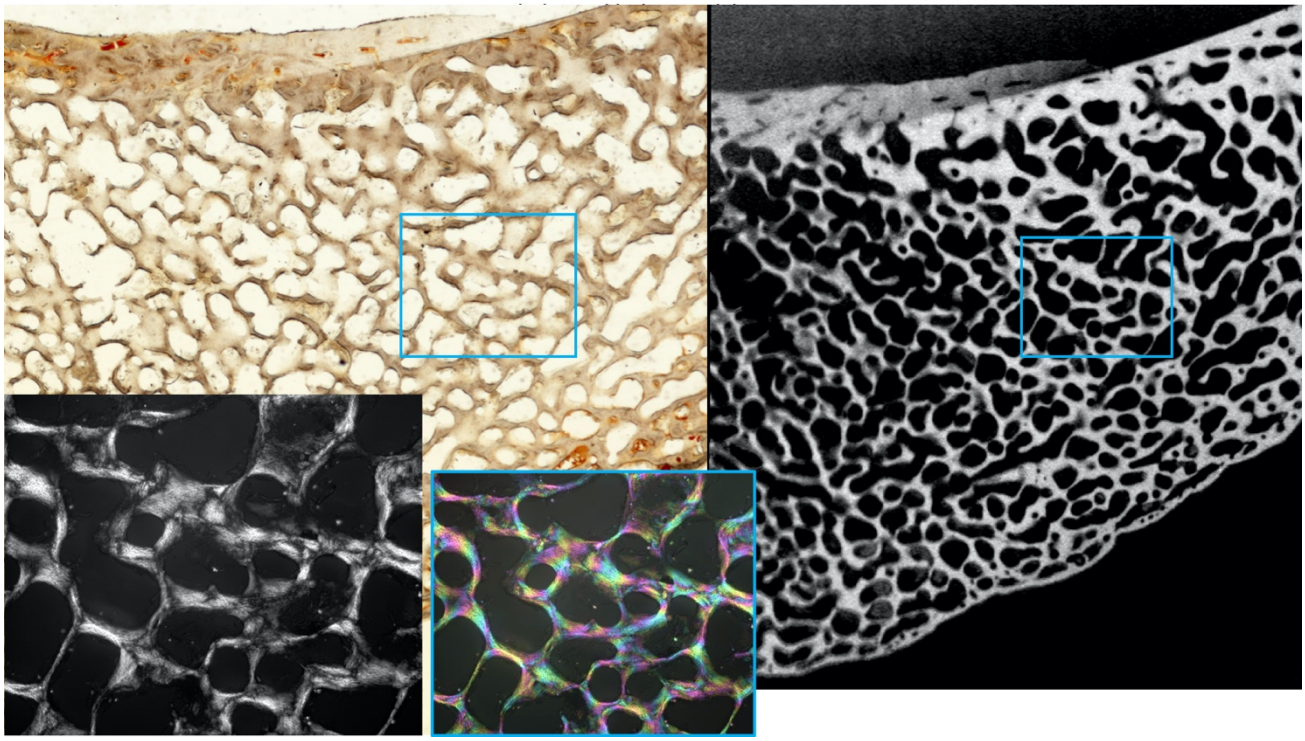

Figure 2: Good correlation between optical microscopy and XMT in a ground section of trabecular bone in a narwhal mandible. Top left is transmitted light VueScan image, Right is XMT, bottom left is PLM, bottom center is color circle sequence of 12 PLM images at 7.5° rotation intervals [see ref. 23]. Marked fields which show the same area in each are 3mm wide. This is an example of material which would probably be impossible to reproduce today due to CITES rules. [CITES: Convention on International Trade in Endangered Species of Wild Fauna and Flora is an international agreement between governments which aims is to ensure that international trade in specimens of wild animals and plants does not threaten the survival of the species]. This slide was produced from tissue donated by the late Ed Mitchell of the Canadian Dept of Fisheries and Oceans (St Anne de Bellevue, PQ, Canada) from material from indigenous Canadian Inuit narwhal hunting.

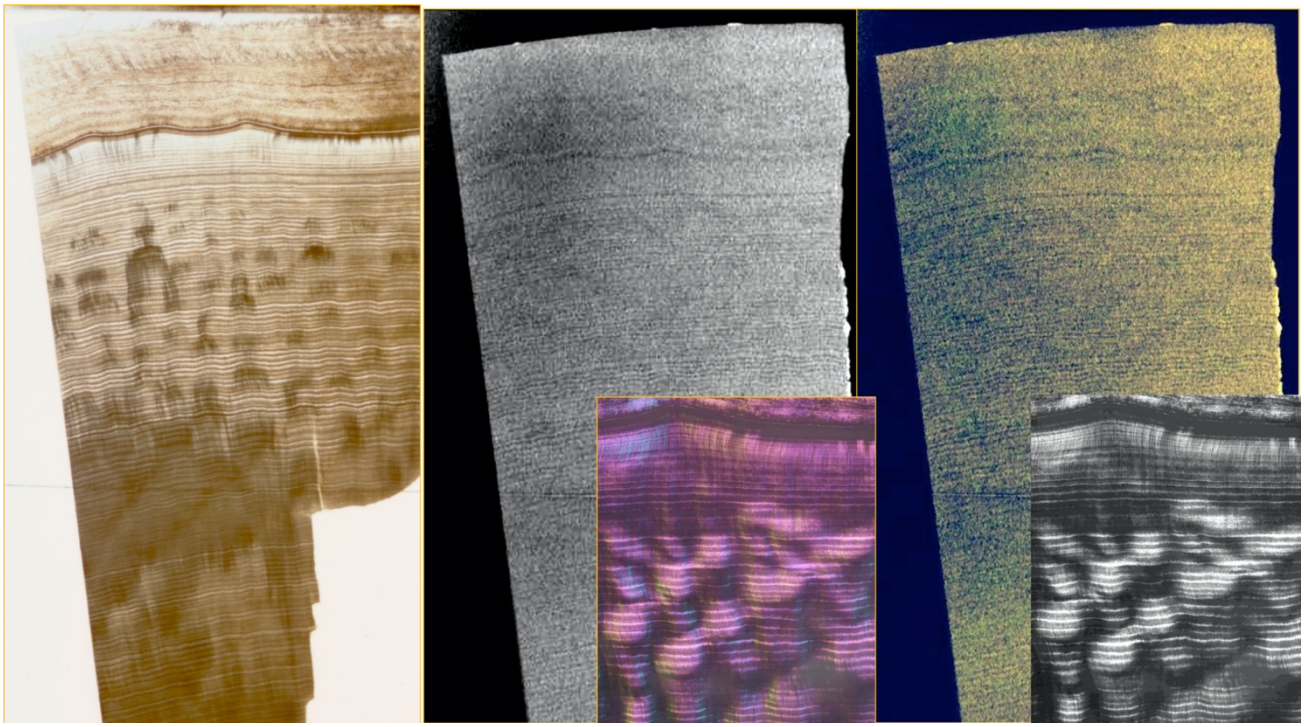

Figure 3: African elephant Ivory TS. Top left is ordinary transmitted light VueScan image. Top center is SUM of 3 XMT slices. Top right shows XMT of 2 slices as a color composite; the SUM in Red, the MAXimum in Green, and the MINimum in Blue. Greatest width of sample is 7.5mm. The inset PLM images below are 3mm high. The colored image is color circle sequence of 12 PLM images at 7.5° rotation intervals [see ref. 23]. The monochrome image at bottom right shows the SUM of the same 12 images, which is essentially the same as a circularly polarized light image. All the images show very clear incremental growth lines and the 'chequer board' pattern which results from oscillatory motions of the dentine-forming cells (odontoblasts) during development. [see Figure 7 in ref. 27].

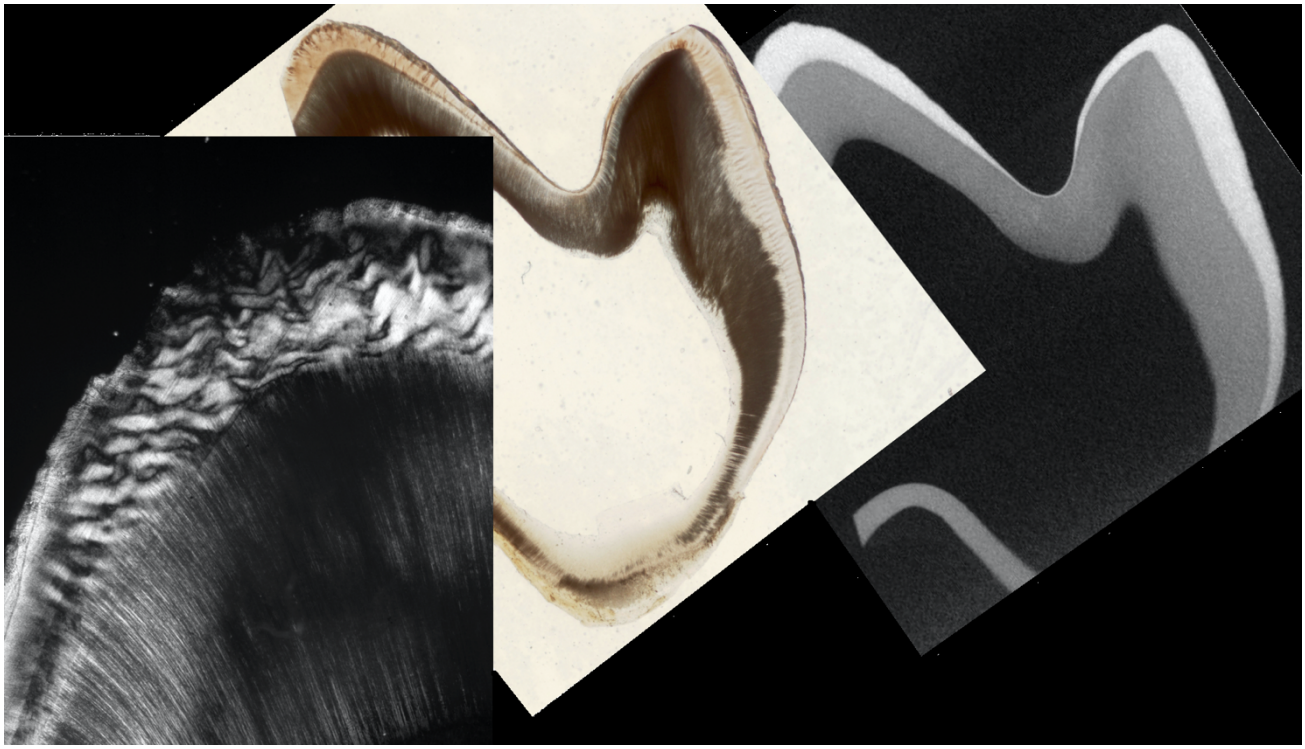

Figure 4: Dog carnassial tooth, longitudinal mesio-distal ground section, width 9.5mm. The XMT image at top right shows the SUM of 2 slices and more clearly delineates the thin enamel layer between the two cusps of the tooth. The ordinary transmitted light VueScan image at center shows most dentine as dark due to light scattering from air retained in the dentine tubules. The single PLM image at left (field height = 3mm) shows the very strongly marked decussation of the enamel prisms [Hunter-Schreger bands, diazones, parazones] - essentially due to the different directions of orientation of bundles of elongated hydroxyapatite crystals[27], which are not seen in XMT.

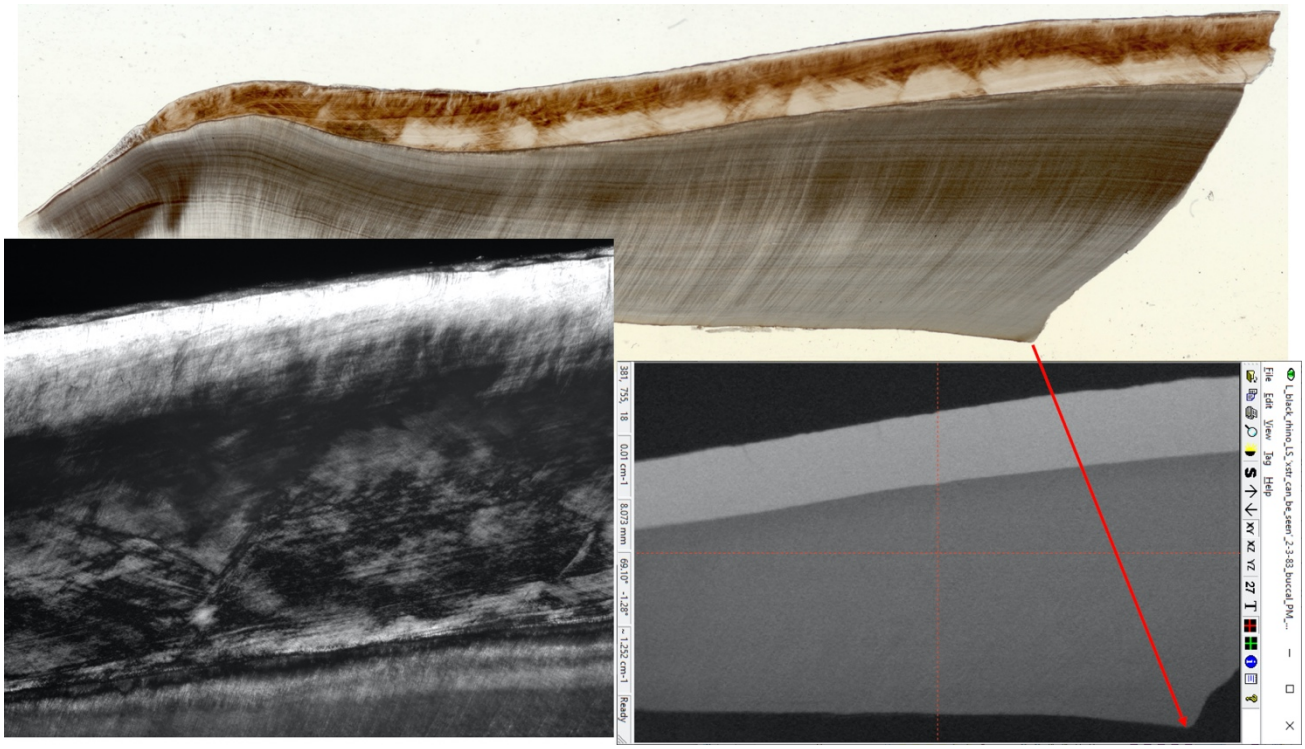

Figure 5: A longitudinal ground section showing the buccal side of a black rhino premolar. VueScan ordinary transmitted light image at top, field width 33.5mm. Single PLM image bottom left, field width 3mm. Slice 18 of the XMT data in TomView at bottom right, field height 9mm. A major feature of interest here is the vertical decussation[27] of the enamel prisms in the inner half to two-thirds on the enamel, very clearly seen in both ordinary and polarized light microscopy. XMT shows that this has nothing to do with the degree of mineralization in the completed enamel.